Amperometric Environmental Phosphate Sensor

Yuanyuan Lu[1], Xiuting Li[2], Danlei Li[1], and Richard G. Compton[1*]

[1] Department of Chemistry, Physical and Theoretical Chemistry Laboratory, Oxford University, South Parks Road, Oxford OX1 3QZ, UK

[2] Institute for Advanced Study, Shenzhen University, Shenzhen, Guangdong 518060, China

* Corresponding author：Richard G. Compton, Email: richard.compton@chem.ox.ac.uk

ABSTRACT: We report a novel amperometric sensor for aqueous phosphate ions in freshwater systems based on the reductive square wave voltammetry of molybdate (VI) anions immobilized within a chitosan matrix deposited on a glassy carbon electrode. A sensitivity of 4.4±0.1 μA/μM was realized together with a LOD of 0.15 μM. The sensor was insensitive to chloride and nitrate ions below threshold concentration of 1.0 mM respectively. Analytical measurements were successfully made in authentic samples of tap and pond water.

KEYWORDS: Phosphate, Molybdate (VI) reduction, Chitosan, Square wave voltammetry, Detection in fresh water

Phosphate anions are one essential constituent of living systems, which not only play an important role in biological systems but also cause detrimental effects in aquatic ecosystems [1, 2]. Excessive inorganic phosphate anions created from unscientific fertilization in farmland soil pass into local water systems through surface and underground runoff, resulting in eutrophication causing widespread water-quality problems, now widely recognised[3, 4]. The US Environmental Protection Agency (EPA) has reported the Federal criteria limit[5] for phosphate of 0.1 ppm, 0.05 ppm and 0.025 ppm in rivers, streams entering lakes and lakes/reservoirs respectively. Therefore, developing simple, sensitive and cost-effective approaches for phosphate analysis in aqueous solutions meets a need.

Various analytical techniques have been applied to detect the concentration of phosphate in environmental, clinical, industrial and biological samples, such as chromatography[6, 7], optical fluorescence[8, 9], colorimetry[10, 11] and spectrophotometry[12, 13]. Although those techniques are highly sensitive and selective, all of them require skilled personnel, large, non-portable expensive instrumentation, and complex measurement procedures. Many features including the excellent sensitivity, rapid analysis time and cost effectiveness of electrochemical techniques[14] make them very attractive for quantitative phosphate analysis. Various designs of electrochemical sensors have been reported based on the electrochemical methods of potentiometry[15, 16] conductometry[17, 18] and amperometry[15,16] for the detection and quantification of trace phosphate.

In principle potentiometric sensing should be a simple electrochemical approach and ion selective sensors (ISEs) have been developed [19-21]. However[22], the realization of high sensitivity within the operable concentration detection range of the phosphate anions is problematic since a triply charge anion shows one third of the Nernstian sensitivity of that of a singly charged anion and, furthermore, the response of phosphate ISEs is strongly pH dependent as the speciation within the solution changes with the formation of $H_2PO_4^-$ and HPO_4^{2-} as well as PO_4^{3-}. Moreover, the hydrophilicity and the size of the phosphate anion make it challenging to design a phosphate selective membrane, which precludes the use of size-exclusion principles for increased selectivity[23]. As a result, few phosphate sensors have become commercially available and attention has shifted to voltammetric (amperometric) sensing.

The major issue for the amperometric detection of phosphate results from the structure of the orthophosphate ion. To be specific, it has been suggested the central P atom covalently bonded to four oxygen atoms creates a hydrophilic sphere around the anion and results in a high enthalpy of hydration,

which makes it electrochemically inactive to reduction and hence difficult to be detected[24] whilst the oxidation state of the P atom makes it inert to oxidation. Thus, in order to be detectable a chemical derivatisation of phosphate is typically required. In particular many reported electrochemical methods for phosphate detection are based on the electrochemical reaction of a phosphomolybdic complex created in situ by using screen-printed electrodes modified with preloaded reagents or even enzymatic systems (shown in Table S1). These detection strategies are usually coupled with complicated and costly preparation procedure, limited electrode lifetimes and high detection limits. The development of a facile, cheap, sensitive electrochemical methodology for the detection of phosphate remains a significant and worthwhile challenge.

In this paper, we present the electrochemical detection of phosphate in aqueous solutions at an ammonium molybdate tetrahydrate (AMT)-chitosan modified glassy carbon macro electrode (AMT-CS-GCE) using cyclic voltammetry (CV) and square wave voltammetry (SWV). The reductive behavior of solution-phase molybdate (VI) anions and phosphate was first investigated via CV. For phosphate detection, we used the enhancement of the observed Mo reduction peaks seen in the presence of phosphate for which an electrocatalytic mechanism is suggested. For the creation of a practical sensor, chitosan was adopted to immobilize the probe molybdate anions onto an electrode surface. The electrochemical response of the sensor was investigated via CV and SWV respectively, and it was found that SWV showed a significantly improved detection sensitivity compared with CV by reducing the effect of capacitative background currents[25]. The method was optimized for detection at pH 2 after simple sample acidification but also shown to be valuable as a reagent free sensor for environmental use at around pH 7, where an application of the manufactured sensor for quantifying phosphate concentration in real water samples was presented.

■ EXPERIMENTAL SECTION

Chemicals and Reagents. All chemicals were of analytical grade and were used as received without any further purification. Ammonium molybdate tetrahydrate (AMT, 99%) was purchased from Alfa Aesar. Potassium Phosphate Monobasic (KH_2PO_4) and Chitosan (MW=100,000) were purchased from Macklin. Acetic acid and Sulphuric acid (H_2SO_4) were obtained from Sinopharm Chemical Reagent Co., Ltd. Potassium sulfate (K_2SO_4), Potassium chloride (KCl) , Potassium nitrate (KNO_3) and Potassium hydroxide (KOH) were purchased from Sigma-Aldrich. All solutions were

prepared using ultra-pure water at a resistivity of 18.2 MΩ cm at 298K (KMD-SHZ, CD Haochun Inc., China).

Theoretical Calculations of Speciation. The distribution diagrams for Molybdenum(VI) (Mo(VI)) were obtained in the pH range 0 to 7 and for total Mo concentrations of 1 mM and 8 mM using Hydra/Medusa software[26] based on the formation conditions of different Mo (VI) complexes H_2MoO_4, $H_3MoO_4^+$, $HMoO_4^-$, MoO_4^{2-}, $Mo_7O_{24}^{6-}$. The distribution diagrams for orthophosphate were similarly obtained in the pH range 0 to 8 again using Hydra/Medusa to identify the relevant concentrations of PO_4^{3-}, HPO_4^{2-}, $H_2PO_4^-$ and H_3PO_4.

Last, based on the equilibria and associated equilibrium constants reported for the formation of the various molybdophosphate complexes[27] from Mo(VI) complexes and orthophosphate species as summarized later in this paper, the speciation in solutions containing both Mo(VI) and phosphates was modelled for different total concentrations of uncomplexed phosphate (0.01 mM to 10.0 mM) for total Mo(VI) concentrations of 8mM using Hydra/Medusa. In all cases, the distribution diagrams of Mo (VI) or P containing species were generated as a function of pH.

Electrochemical apparatus and methods. All electrochemical experiments were carried out in a Faraday cage at 298K using an EC-lab potentiostat (Biologic Science Instruments, France). The CV and SWV measurements were performed using a standard three-electrode system with a glassy carbon macro electrode (GCE) as the working electrode (diameter of 3.02 ± 0.005 mm). A saturated calomel electrode (SCE, SH Xianren Inc., China) was used as the reference electrode and a graphite rod as the counter electrode. Prior to the experiments, the GCE was polished carefully using alumina with decreasing particle sizes of 1.0, 0.3 and 0.05 μm (CH Instruments Inc., China) in turn on soft lapping pads (Buehler, UK), followed by rinsing with ultra-pure water and drying with nitrogen.

Analytical Procedures. KH_2PO_4 stock solutions of 1.0 mM were prepared with 0.05M K_2SO_4 and standard working solutions at different KH_2PO_4 concentrations of 0.01, 0.05, 0.1, 0.2, 0.3, 0.4, 0.6, 0.8, 1.0, 2.0 and 5.0 μM were then obtained by diluting the stock solution with 0.05 M K_2SO_4 solution (pH=2, adjusted by H_2SO_4), 0.05 M K_2SO_4 solution (pH=5.8, without acid or alkali addition) or 0.05 M K_2SO_4 solution (pH=7.8, adjusted by KOH) respectively.

For the CV experiments on the study of Mo (VI) reduction in the absence and presence of phosphate, the GCE was first placed in 0.05M K_2SO_4 solution (pH =2, adjusted by small additions of

0.5M H_2SO_4) containing 0, 50 and 100 μM KH_2PO_4 and 8 mM ammonium molybdate (VI) tetrahydrate. Prior to the measurements, the solutions were bubbled with N_2 to remove the dissolved oxygen. The potential window was chosen to be 0.5 to −1.0 V and 0.5 to −0.1 V respectively, the voltammograms were recorded at different scan rates (25, 50, 100, 200, 400 mVs^{-1}).

For voltammetric experiments to detect phosphate, a novel ammonium molybdate (VI) tetrahydrate-Chitosan modified electrode (AMT-CS-GCE) was fabricated. The drop-cast suspension was prepared by dissolving 0.05 g chitosan in 10 mL 0.1M acetic acid then slowly mixing with 4.0 g ammonium molybdate (VI) tetrahydrate followed by constant stirring for 12 hours. The freshly polished GCE was modified by drop casting 2 μL of ammonium molybdate (VI) tetrahydrate-Chitosan suspension, and the modified electrode was then dried under vacuum.

To investigate the electrochemical response in the presence of phosphate with different concentration, CVs were performed by immersing an AMT-CS-GCE in degassed solutions containing 5, 10, 20, 40 and 80 μM KH_2PO_4 in 0.05M K_2SO_4 (pH=2) from 0.5 V to −0.1 V at a scan rate of 100 mV s^{-1}. The effect of pH was also investigated experimentally: CVs at an AMT-CS-GCE were obtained at a scan rate of 0.1 V s^{-1} in a solution containing 10 μM KH_2PO_4 in 0.05M K_2SO_4 at different pH values (1.5 to 5.5) which were adjusted using different concentrations of H_2SO_4 and the potential window was adjusted to accommodate the shift in potential to observe the oxidation and reduction peaks.

The phosphate detection was realized using SWV where the AMT-CS-GCE was immersed in solutions containing 0, 0.3, 0.6, 1 and 2 μM KH_2PO_4 in 0.05M K_2SO_4 (pH=2) and solutions containing 0, 0.05, 0.1, 0.2, 0.4, 0.6 and 0.8 μM KH_2PO_4 in 0.05M K_2SO_4 (pH=5.8, without acid or alkali addition) respectively under degassed conditions as above. An oxidizing pulse was first applied at a potential of 0.6 V for 10 s to generate hydrogen ions via electrolysis of water to make the electrode environment more acidic, then SWV experiments were carried out from 0.6 V to -0.1 V at a scan rate of 25 mVs^{-1}, with a pulse height of 25 mV and an accumulation time of 3 minutes.

Real sample analysis. The authentic water samples used in this work were either laboratory tap water or natural pond water from Wenshan lake both located in Shenzhen University, China (113.93 °E, 22.54 °N). Pond water samples were filtered using filter paper (pore size: 1 μm) to remove solid impurities before further analysis.

Tap water was directly used as the solvent to prepare a 0.05 M K_2SO_4 solution (pH=2). The pond water was diluted 10 times with a 0.05 M K_2SO_4 solution (pH=2). The AMT-CS-GCEs were used in the real sample solutions for SWV analysis at a scan rate of 25 mV s^{-1} with a pulse height of 25 mV and an accumulation time of 3 minutes. The potential was stepped from 0.6 V to -0.1 V and an oxidizing pulse was first applied at a potential of 0.6 V for 10 s before the SWV was conducted. The concentrations of phosphate were determined by the standard addition method and the accuracy was assessed by a recovery test.

■ RESULTS AND DISCUSSION

We first investigated the cyclic voltammetry at GC macro electrodes in acidified molybdate (VI) solutions in the absence or presence of phosphate and a detection mechanism for phosphate involving an electrochemical catalytic process was proposed. Second, the analytical responses using CV and SWV for the detection of phosphate at AMT-CS-GCEs were studied. Finally, as a proof of concept, we applied AMT-CS-GCEs to quantify phosphate concentrations in real samples.

Speciation of Mo (VI) in aqueous solution. The equilibration of Molybdenum (VI) in aqueous solution involves reactions between MoO_4^{2-} and hydrogen ions and depends on the Molybdenum concentration which controls the extent of condensation reactions to form species containing more than one Mo atom. The distribution diagrams of the different Mo (VI) species as a function of concentration and pH were shown in Fig.S1. Molybdate and protons were produced by decomposition of $Mo_7O_{24}^{6-}$ utilized as the analyte in this work; the electrolyte solutions studied were prepared according to the following reaction equation (1): $Mo_7O_{24}^{6-}+4H_2O \rightleftharpoons 7MoO_4^{2-}+8H^+$ (1).

The electrochemical study of Mo (VI) in the absence of phosphate. Cyclic voltammograms were scanned from 0.5 V to -0.1 V at bare GCEs in 0.05 M K_2SO_4 (pH=2, see Experimental section) in the presence of 8 mM Mo (VI) or not at 400 mVs^{-1}. As depicted in Fig. 1(A), there were two reduction peaks observed at 0.20 V and 0.05 V only in the presence of Mo (VI) into 0.05 M K_2SO_4 (pH=2). These reduction peaks were labelled as $Peak_1$ and $Peak_2$ and the areas (charge) were the same for both cathodic and anodic peaks, the origins of which were discussed below.

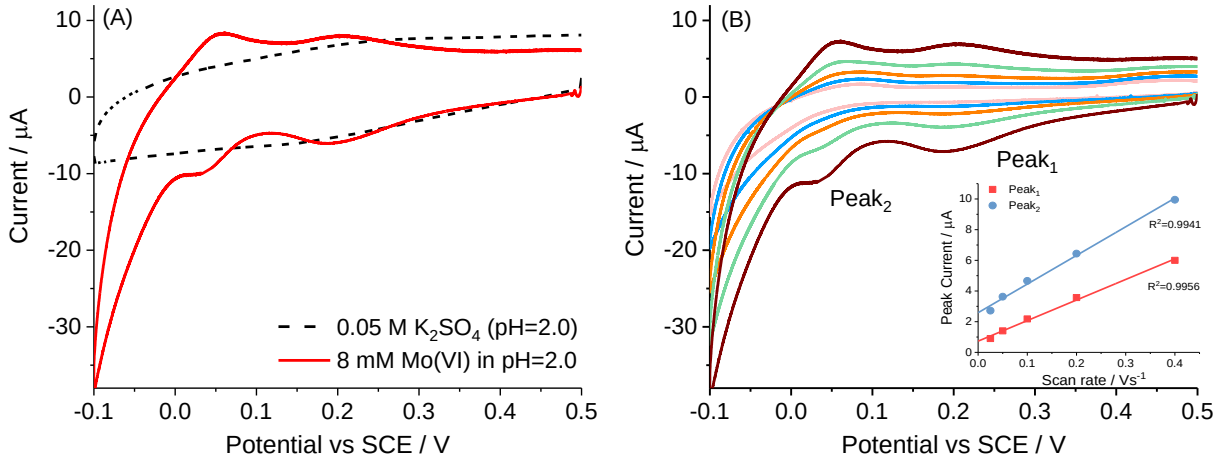

Figure.1 Electrochemical characterization of solution phase Mo (VI) in 0.05 M K_2SO_4 solution (pH 2.0) under degassed conditions: cyclic voltammograms at GCE of (A) background (black dashed line) and 8 mM Mo (VI) (red solid line) in the potential window from 0.5 V to -0.1 V at a scan rate of 400 mVs^{-1} ; (B) 8.0 mM Mo (VI) in the potential window from 0.5 V to -0.1 V at variable scan rates of 25 (pink), 50 (blue), 100 (orange), 200 (green) and 400 (brown) mV s^{-1} (Inlay: plot of peak current of $Peak_1$ (red) or $Peak_2$ (blue) as a function of scan rate).

Cyclic voltammograms were recorded at scan rates in the range of 25–400 mVs^{-1} in 8mM Mo (VI)/0.05 M K_2SO_4 (pH=2) (Fig. 1(B)). As shown in inlay of Fig.1(B), the currents of $peak_1$ and $peak_2$ scaled linearly with the scan rate from 25 to 400 mVs^{-1} indicating the electrochemistry of surface bound Mo species. The peak to peak separation ($\Delta E_{pp}=|E_{p(anodic)}-E_{p(cathodic)}|$) for $peak_1$ and $peak_2$ were calculated to be 0.015 $\pm$ 0.002 V and 0.023 $\pm$ 0.003 V respectively which were close to the ideal value of zero for a reversible surface process and also roughly constant at different scan rates from 25 mV s^{-1} to 400 mV s^{-1}, indicating the reduction of Mo (VI) occurring at $Peak_1$ and $Peak_2$ were both electrochemically reversible processes. The formal potentials for each redox process was obtained to be 0.200 ± 0.002V ($peak_1$) and 0.047 ± 0.003V ($peak_2$) from the midpoint potential ($E_{formal} = \frac{E_{p(anodic)}+E_{p(cathodic)}}{2}$). The surface coverages (Γ) were obtained via:

$$\Gamma = \frac{Q}{nFA} \qquad (2)$$

where Q is the charge passed ($Q = \frac{S_{peak\ area}}{v}$, C), n is the number of electrons transferred (n=1), F is the Faraday constant (96485 C mol^{-1}), A is the electrode area (7.1×10^{-2} cm^2). The raw cyclic voltammograms were background corrected prior to calculation of the coverage as shown in the S3.

Accordingly, in 0.05 M K_2SO_4 (pH=2), based on the one-electron reduction of Mo (VI) to Mo(V), the average surface coverage of $Peak_1$ and $Peak_2$ were estimated to be $(7.6\pm1.8)\times10^{-10}$ mol cm^{-2} and $(2.1\pm1.3)\times10^{-11}$ mol cm^{-2}, respectively. Comparing the average estimated distance between the particles (~$(10^{-8}$-$10^{-7})$ cm/per particle) and $Mo_7O_{24}^{6-}$ ion particle size (~9×10^{-8} cm)[28], the Mo (VI) adsorption is considered to be approximately monolayer coverage.

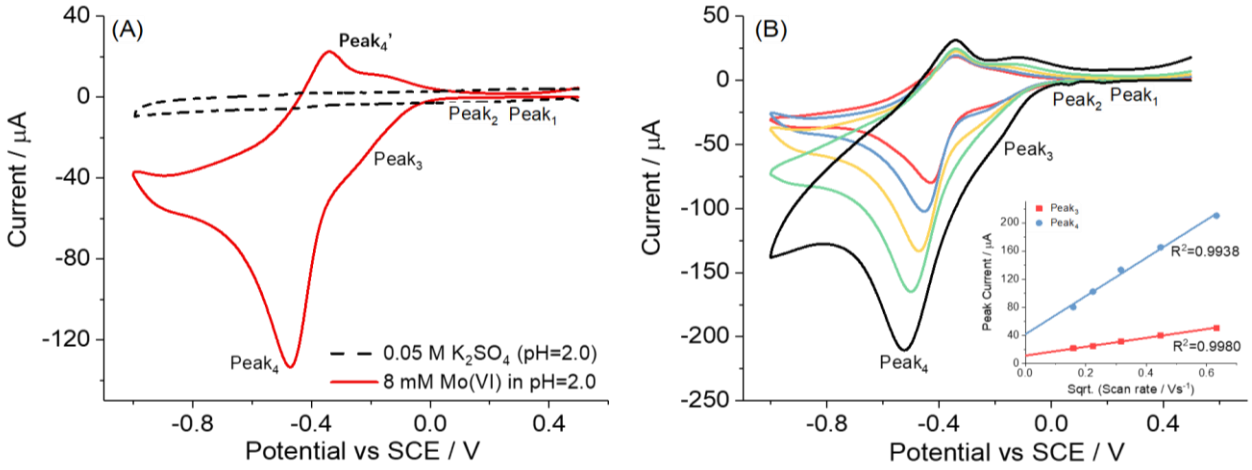

Figure.2 Electrochemical characterization of solution phase Mo (VI) in 0.05 M K_2SO_4 solution (pH 2.0) under degassed conditions in the potential window from 0.5 V to -1.0 V: cyclic voltammograms at GCE of (A) background (black line) and 8 mM Mo (VI) (red line) at a scan rate of 100 mV s^{-1} ; (B) 8.0 mM Mo (VI) at varying scan rates of 25 (red), 50 (blue), 100 (yellow), 200 (green) and 400 (black) mVs^{-1} (Inlay: plot of peak current of $Peak_3$ (red) or $Peak_4$ (blue) as a function of scan rate).

Having reported the voltammetry of 8 mM Mo (VI) occurring at bare GCEs in the potential window from 0.5 V to -0.1 V, we next investigated the electroreduction process of 8 mM Mo (VI) in 0.05 M K_2SO_4 (pH 2.0) across the full potential ranges from 0.5 V to -1.0 V (shown in Fig.2). Fig.2 (A) shows the response with (red line) or without (black line) the Molybdenum species at a scan rate of 100 mV s^{-1}. Four reduction peaks were observed at 0.20V, 0.03V, -0.31V and -0.47V marked as $Peak_1$, $Peak_2$, $Peak_3$ and $Peak_4$. The electrochemical behavior of $Peak_1$ and $Peak_2$ have been revealed as surface bound features in Fig.1 and the discussion thereof above, while the peak currents of reduction $Peak_3$ at -0.31 V and $Peak_4$ at -0.47 V were found to exhibit a linear relationship with the square root of scan rates from 25–400 mVs^{-1} (Inlay of Fig.2 (B)) respectively, suggesting $Peak_3$ and $Peak_4$ are diffusion-controlled. The reverse voltammetric scan showed a peak ($Peak_4$') at -0.34 V which is related to $Peak_4$. The peak-to-peak separation ($\Delta E_{pp}=|E_{p(anodic)}-E_{p(cathodic)}|$) for Peaks 4 and 4' was scan rate dependent and in the potential range of 0.1–0.2 V suggesting a Peaks 4 and 4' relate to

a solution phase electrochemically quasi-reversible process.

The valence states of the Mo based redox couples involved in $Peak_1$, $Peak_2$, $Peak_3$ and $Peak_4$ were assigned based on literature reports. X-ray photoelectron spectroscopy (XPS)[29] identified Mo(V) as the electrochemical reduction product for both $Peak_1$ and $Peak_2$, which were believed to arise due to reduction of two different forms (or adsorption sites) of adsorbed Mo (VI) species. The presence of reverse peaks in the anodic scan shown in Fig.1(B) suggested that the species were retained on the surface after reduction. By studying cyclic voltammetric behavior of Mo(VI) at GCE in the potential range from 0.5 V to -1.0 V, K.Chandarasekara Pillai et.al [30] also suggested that the electron transfer process corresponding to $Peak_4$ in Mo (VI) had a solution phase diffusion-controlled mechanism but the $Peak_3$ was influenced by reactant adsorption especially at high scan rates. In summary, K.Chandarasekara Pillai et.al thought that all four peaks were all attributable to the Mo (VI) reduction to Mo (V) in 0.1M H_2SO_4 but in four different chemical and/or adsorbed forms. We suggested that $Peak_3$ lying at -0.31 V was likely to be an adsorptive pre-wave of $Peak_4$ and most Mo (VI) in solution phase could be postulated to take part in the reduction reaction at $Peak_4$ following a one-electron electrochemically quasi-reversible step. The whole process can be represented as Eqs. (3)-(6):

$$(Mo\ (VI)_A)_{ads} + e^- \rightarrow Mo\ (V)_{ads} \qquad Peak_1 \qquad (3)$$

$$(Mo\ (VI)_B)_{ads} + e^- \rightarrow Mo\ (V)_{ads} \qquad Peak_2 \qquad (4)$$

$$(Mo\ (VI)_C)_{sol} + e^- \rightarrow (Mo\ (V)_C)_{ads} \qquad Peak_3 \qquad (5)$$

$$(Mo\ (VI)_D)_{sol} + e^- \rightarrow (Mo\ (V)_D)_{sol} \qquad Peak_4 \qquad (6)$$

Note that the subscript 'ads' means that the species is adsorbed and that different adsorption sites are speculated to apply to Peaks 1, 2 and 3.

Speciation of phosphate as a function of pH. Using the known chemical equilibrium constants of the various phosphate species[31], the distribution diagram of orthophosphate as a function of pH (0-8) was calculated using Hydra/Medusa (Fig.S3). The speciation of phosphate among various species in aqueous solution was strongly dependent on solution pH but $H_2PO_4^-$ was the major species when the pH range was within $2.1 \leq pH \leq 7.2$, while H_3PO_4 and HPO_4^{2-} were predominant at pH below 2.1 and above 7.2 respectively.

Species distribution of Mo and P containing compounds as a function of pH for various total

phosphate concentrations. In order to clarify the speciation in solutions of Mo(VI) and phosphate, the distribution diagrams of Mo(VI) and P containing compounds as a function of pH from 0 to 7 were generated respectively when $[Mo(VI)]_{Total}$=8 mM while varying the total phosphate concentration $[PO_4^{3-}]_{TOT}$ from 0.1 μM to 0.01, 0.1, 1.0 and 10.0 mM (see S5). It was noted that the distribution diagrams were unchanged for total phosphate concentrations $[PO_4^{3-}]_{TOT}$ below 0.01 mM as shown in Fig.S4-3. By way of summary, Table S3-1 showed the changing composition of an 8 mM Mo solution as the amount of phosphate was altered based on the fraction distribution of Mo containing species (Fig.S4-1) and P containing species (Fig.S4-2) at pH=2 with a [Mo(VI)] total concentration of 8 mM when $[PO_4^{3-}]_{TOT}$ was changed from 0.01 mM to 0.1, 1 and 10 mM. The conditions under which individual concentrations of key species are maximal were given in Table S3-2. It is clear that the distribution of Mo (VI) and P containing complexes are very sensitive to the Mo (VI)/P concentration ratio and are strongly pH dependent. In the following, the Hydra/Medusa program and database were used to correlate electrochemical signals with the speciation and hence assign voltammetric peaks.

Electrochemical behavior of Mo (VI) catalyzed reduction of phosphate studied via cyclic voltammetry. The electro-reduction of Mo (VI) across the full potential ranges of interest was investigated by scanning voltammograms between 0.5 V to -1.0 V in 8mM Mo (VI)/0.05 M K_2SO_4 (pH 2.0) in the presence of 0, 50 and 100 μM KH_2PO_4. As can be seen in Fig. 3(A), five peaks were observed at 0.20 V, 0.03 V, -0.31 V, -0.47 V and -0.82 V labelled $Peak_1$, $Peak_2$, $Peak_3$, $Peak_4$ and $Peak_5$ in the presence of KH_2PO_4. It was noted that the first four peaks ($Peak_{1-4}$) appeared at similar potentials as those in the absence of KH_2PO_4 while $Peak_5$ was observed only in the presence of 0.05 and 0.1 mM KH_2PO_4. It was also found that currents of $Peak_1$, $Peak_2$, $Peak_3$ and $Peak_5$ increased but the $peak_4$ current decreased with the continuous addition of KH_2PO_4.

Fig.3(B) showed the CV response over the narrower potential range of 0.5 V to -0.1 V for concentrations of KH_2PO_4 of 0, 0.05, 0.1, 0.2, 0.5 and 1.0 mM. $Peak_1$ was only slightly influenced by the addition of KH_2PO_4 (see Fig.3(C)) but $Peak_2$ was seen to develop a shoulder (labelled peak 2*) and the overall $Peak_2$ + $Peak^*_2$ feature grew in size developing a current plateau rather than a peak at higher scan rates. These features signaled a possible catalytic process and probably also an enhanced adsorption. It was noted that the current of $Peak_2$ and $Peak^*_2$ increased linearly with increasing KH_2PO_4 concentration over the range studied (Fig.3(B)) and $Peak^*_2$ assigned as a pre-peak of $Peak_2$

gradually disappeared as the scan rate was increased to 200 mV s^{-1}. Meanwhile the current values of $Peak_1$ and $Peak_2$ had a linear relationship with the scan rate from 25 mV s^{-1} to 400 mV s^{-1} respectively again suggesting their surface bound nature (Fig.3(D)). The enhancement of both forward and reverse peaks 1 and 2 in the presence of phosphate suggested that there was a chemical reaction of the phosphate with the Mo (VI) species, leading to the formation of species which showed enhanced adsorption especially in the case of $Peak_1$. The possible species included $PMo_{12}O_{40}^{3-}$ and $P_2Mo_{18}O_{62}^{6-}$ which were significant at pH=2 when $[PO_4^{3-}]$ was in the range from 0.01 to 1 mM according to the speciation distribution diagram. The catalytic reaction probably involved Mo(V) reacting with either the phosphate or with Mo-P species via a reaction[32] such as Eqs (7) and (8)

$$(Mo\ (V))_{ads} + PMo_{12}(VI)O_{40}^{3-} \rightarrow Mo\ (VI) + PMo_2(V)\,Mo_{10}(VI)O_{40}^{3-} \quad (7)$$

$$(Mo\ (V))_{ads} + P_2Mo_{18}(VI)O_{62}^{6-} \rightarrow Mo\ (VI) + P_2Mo_2(V)\,Mo_{16}(VI)O_{62}^{6-} \quad (8)$$

The increase of $Peak_3$ currents with the addition of KH_2PO_4 also suggested a possible surface catalytic (EC') process such as:

$$(Mo(V)_C)_{ads} + PMo_2(V)Mo_{10}(VI)O_{40}^{3-} \rightarrow (Mo\ (VI)_C)_{sol} + PMo_4(V)\,Mo_8(VI)O_{40}^{3-} \quad (9)$$

In order to clarify the origins of the Peaks 1-5, Fig.4(A) showed the speciation of Mo (VI) containing compounds over the range of phosphate studied from 0.05 to 1.0 mM, it can be seen that the concentrations of all mono Molybdate species (MoO_4^-, $H_3MoO_4^+$, H_2MoO_4 and $HMoO_4^-$) gradually decreased when $[PO_4^{3-}]$ was increased from 0.05 mM to 1.0 mM. In contrast, the concentrations of $PMo_{12}O_{40}^{3-}$ and $PMo_{11}O_{39}^{7-}$ stayed stable when $[PO_4^{3-}]$ was lower than 0.7 mM and then started to decrease slightly. In contrast the concentration of $P_2Mo_{18}O_{62}^{6-}$ increased over the whole range of phosphate. In particular it can be seen from Fig.4(B) and (C) that the peak currents associated with $Peak_4$ and new $Peak_5$ seen in the presence of KH_2PO_4 correlated with the calculated trends in H_2MoO_4 and $PMo_{12}O_{40}^{3-}$ concentration respectively when the $[PO_4^{3-}]_{TOT}$ was set to be 0, 0.05, 0.07 and 0.10 mM, suggesting that the electroreduction of H_2MoO_4 was observed at $Peak_4$ and electron-reduction product of $PMo_{12}O_{40}^{3-}$ was responsible for this diffusion controlled electroreduction $Peak_5$ (Fig.4(D)).

In the following we sought to build on the observations above that peaks 1 and, especially, 2 were responsive to the solution phosphate concentration. We noted that these involved adsorbed Mo (VI) and that on a GCE surface the extent of adsorption was strictly limited and constrained by the

geometric area of the electrode. In order to increase the amount of Mo (VI) available for detection of phosphate, we sought to immobilize the Mo (VI) species in a matrix of chitosan. The structure of the latter was shown in Fig 5(A). Since the amino groups in chitosan have a pKa value of ~ 6.5 at 298K[33] they are protonated at acidic pH and the resulting cationic groups in principle can bind anions of Mo(VI). In addition chitosan is known to show good adhesion to electrodes and excellent film forming ability[34, 35].

Molybdate (VI) was immobilized on GC macroelectrodes by drop casting a certain amount of a chitosan-ammonium molybdate (VI) tetrahydrate (AMT) suspension dissolved in 0.1M acetic acid to create a Mo (VI)-Chitosan modified electrode (AMT-CS-GCE). Then to explore the electrochemical response of AMT-CS-GCE, three GC electrodes after different treatments were compared: 1) an unmodified GCE after polishing, 2) chitosan immobilized on a bare GCE; and 3) an AMT-CS-GCE as described in the Experimental section. These were separately placed in 0.05 M K_2SO_4 (pH=2.0) in the absence and presence of 0.01 mM KH_2PO_4. After N_2 bubbling as above to remove oxygen, the cyclic voltammograms were recorded in the sweep potential range from 0.50 V to – 0.1 V at a scan rate of 100 mV s^{-1}. As shown in Fig.5(B), in the absence of KH_2PO_4, two reduction peaks were observed at 0.15 V ($Peak_1$) and 0.03 V ($Peak_2$) in 0.05 M K_2SO_4 (pH=2.0) at AMT-CS-GCE (orange curve). The peak to peak separations of $Peak_1$ and $Peak_2$ ($\Delta Epp=|E_{p(anodic)}-E_{p(cathodic)}|$) were calculated to be 0.014 $\pm$ 0.003 V and 0.005 $\pm$ 0.000 V respectively which were close to the ideal value of zero for a reversible surface process, indicating that both peaks 1 and 2 seen at the AMT-CS-GCE were electrochemically reversible processes. Formal potentials were obtained from the midpoint between the reduction and oxidation peak potentials and the values of 0.158$\pm$0.006V ($Peak_1$) and 0.027$\pm$0.003V ($Peak_2$) were obtained. The average charge passed at $Peak_1$ and $Peak_2$ were calculated to be 1.7(±0.3) $\times10^{-6}$ C and 9.3(±3.5) $\times10^{-7}$ C, which were both substantially higher than the charge passed on the surface of only Mo(VI) modified GCE ($Peak_1$: 5.1($\pm$1.2) $\times10^{-7}$ C and $Peak_2$: 4.7(±1.2) $\times10^{-7}$ C) suggesting there were more electroactive Mo(VI) ions adsorbed on the surface probably due to the molybdate (VI) anions bound electrostatically to the $–NH_2$ groups of the Chitosan which were protonated at the pH values used. Then the number of Mo (VI) containing molecules on the surface of AMT-CS-GCE of 1.2(±0.3) $\times10^{9}$ ($Peak_1$) and 6.1(±2.6) $\times10^{8}$ ($Peak_2$) were estimated by using the average charge passed, which was smaller compared to the number of NH_2- groups in the deposited chitosan (~1.5×10^{13}). All above indicated that the molybdate had been successfully

immobilized by chitosan on the surface of GCE and behaved in a similar way as in the solution phase.

We next turned to the analytical response of phosphate at AMT-CS-GCEs by using CV in 0.05 M K_2SO_4 (pH=2.0). The voltammogram recorded by bare GCE (green curve in Fig.5(B)) and chitosan modified GCE (blue curve in Fig.5(B)) containing 0.01 mM KH_2PO_4 showed no reduction peak; Only exposing the modified AMT-CS-GCE to 0.01 mM KH_2PO_4 (black curve in Fig.5(B)), both reduction $Peak_1$ and $Peak_2$ became more apparent at the same potential location compared with those in the absence of KH_2PO_4. It was clear that chitosan trapped the molybdate species and provided the required acidic environment for the electrochemical reactions to occur but had no substantive effect on the response to phosphate.

To achieve the best detection sensitivity, several parameters in cyclic voltammetric behavior were optimized (See S6). The effect of chitosan mass concentration in modification suspension was studied with a fixed 40 g L^{-1} AMT/10 mL 0.1M acetic acid setting the modification amount to be 2 μL. As shown in Fig.S5(A), in the presence of 5.0 μM KH_2PO_4, the response increased initially upon raising the chitosan concentration to 5 g L^{-1} due to the presence of chitosan effectively promoted the stabilization of AMT adsorbed on the surface. However, this effect began to decrease at concentrations higher than 5 g L^{-1} because excess chitosan lowered the electrical conductivity of the film. Therefore, the chitosan mass concentration of 5 g L^{-1} was used for subsequent electrode preparation. Further, when 2 μL of the AMT/chitosan suspension was used for modification, the current of $Peak_2$ in the resulting AMT-CS-GCE was the highest (Fig.S5(B)). The thickness of the modified AMT-chitosan layer was estimated to be 1.4 μm (see S7).

The effect of pH on the performance of AMT-CS-GCEs in respect of the cyclic voltammetric behavior of phosphate was investigated in 10.0 μM KH_2PO_4/0.05M K_2SO_4 (Fig.S5(C)). In the pH range from 1.5 to 5.0, the reduction peaks, $Peak_1$ and $Peak_2$ were seen to shift in the cathodic direction to lower potential values with increasing pH of the electrolyte solution. Further, above pH 2 there was a gradual decrease in the peak sizes which was consistent with the species distribution diagram (Fig.S1) where the monomeric forms ($HMoO_4^-$, H_2MoO_4 and $H_3MoO_4^+$) gradually disappeared in the range $3<pH<5$, and which were likely the dominant species of Mo (VI) in electrochemical reduction processes. This might limit the sensitivity of AMT-CS-GCEs in lower acidic condition.

Next, cyclic voltammograms with respect to phosphate concentration at AMT-CS-GCEs were

further conducted in 0.05 M K_2SO_4 (pH=2.0). Fig.5(C) depicted the cyclic voltammetric response as a function of increasing concentration of KH_2PO_4 with the concentration in the range of 5.0–80.0 μM. The plot of peak height versus phosphate concentration obtained using CV showed a linear relationship in the mentioned range (Inlay of Fig.5(C)). The calibration curves are: $Peak_1$: $I_p(\mu A) = 0.027[PO_4^{3-}]_{TOT}$ (μM) + 2.2 (μA), R^2=0.9685; $Peak_2$: I_p (μA) = $0.093[PO_4^{3-}]_{TOT}$ (μM) +3.6 (μA), R^2=0.9974. The limit of detection (LOD) was found equal to 0.7 μM, calculated as $3\sigma_b/m$ using 10 measurements of the blank (n=10), where σ_b is standard deviation of results obtained in blank solution, m is the slope of calibration curve.

The above demonstrated that the AMT-CS-GCE had the capability to detect the lower concentrations of phosphate in aqueous solutions by CV in respect to the bare GCE, also suggested that the electrochemical reduction of Mo (VI) to Mo (V) happened on the modified electrode were more effectively promoted by catalyzing phosphate reduction. However, to further meet the requirements of trace phosphate analysis in real samples and find out the possibility of reagent-less detection of phosphate at neutral pH, we employed square wave voltammetry (SWV) to reduce the effect of capacitive background current and improve the detection sensitivity in the following.

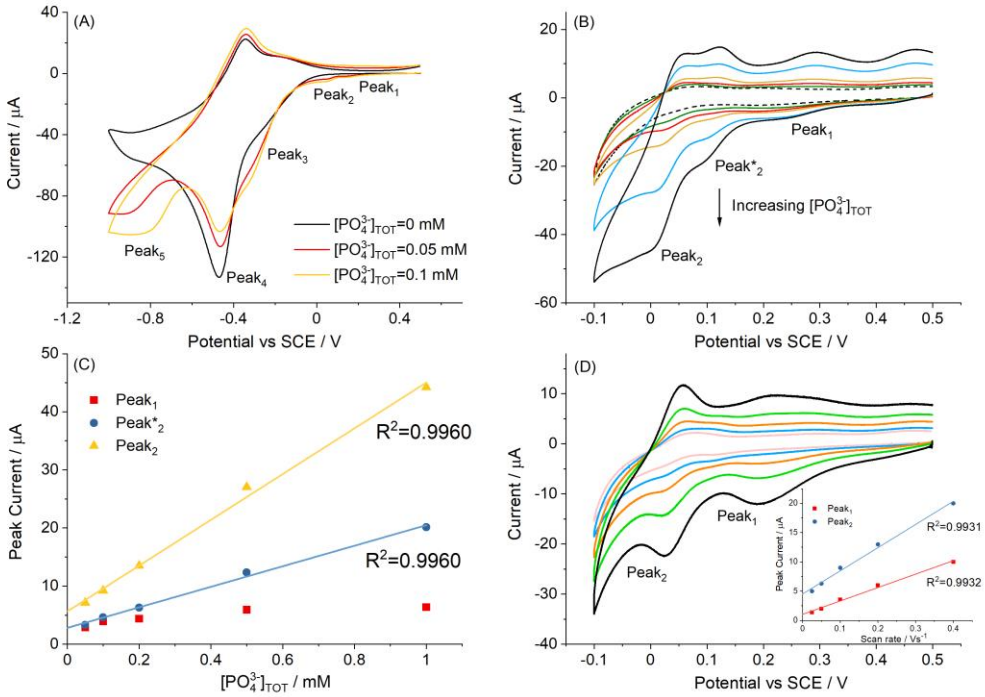

Figure.3 CV at a bare GC macroelectrode of KH_2PO_4 in 8mM Mo (VI)/0.05 M K_2SO_4 solution (pH 2.0) under degassed conditions: (A) cyclic voltammograms of 0, 0.05 and 0.1 mM KH_2PO_4 from 0.5 V to -1.0 V at a scan rate of 100 mVs^{-1}. (B) cyclic voltammograms of a bare GC macroelectrode with 0 mM, 0.05 mM, 0.1 mM,

0.2mM, 0.5mM and 1.0 mM of KH_2PO_4 from 0.5 V to -0.1 V at a scan rate of 100 mV/s; (C) Calibration curve plot showing the peak currents of $Peak_1$, $Peak^*_2$ and $Peak_2$ versus total phosphate concentration at a scan rate of 100 mVs^{-1} ;(D) cyclic voltammograms of 0.1 mM KH_2PO_4 at a bare GC macroelectrode at varying scan rates from 25 mVs^{-1} to 400 mVs^{-1} (Inlay: the plot of $Peak_1$ and $Peak_2$ current as a function of the scan rate)

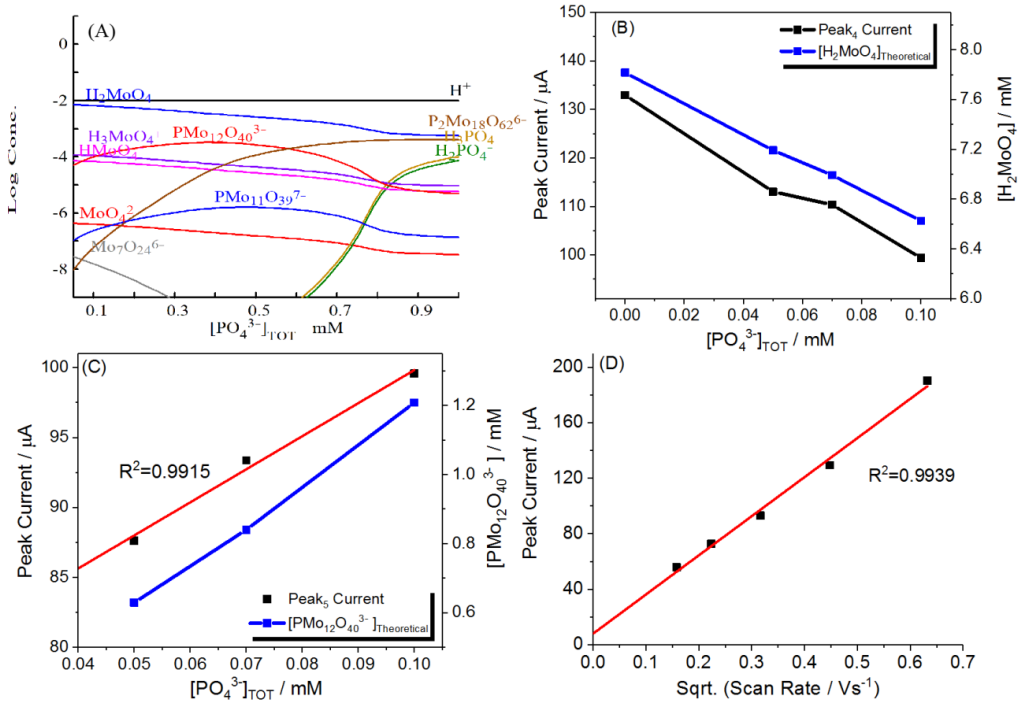

Figure.4 (A) Plot of Log.Concentration of each species (including Mo(VI) and P containing compounds) versus total phosphate concentration, $[PO_4^{3-}]_{TOT}$ from 0.05mM to 1mM in the presence of 8mM Mo(VI) when pH is 2.0; (B) $Peak_4$ current (Left Y-axis) and H_2MoO_4 theoretical concentration (Right Y-axis) as $[PO_4^{3-}]_{TOT}$ changes from 0 mM to 0.1 mM; (C) Correlation of $Peak_5$ current (Left Y-axis) and $PMo_{12}O_{40}^{3-}$ theoretical concentration (Right Y-axis) as a function of concentration of $[PO_4^{3-}]_{TOT}$ changes from 0.05 mM to 0.1 mM;(D) Linear peak current of $Peak_5$ behavior at various scan rates.

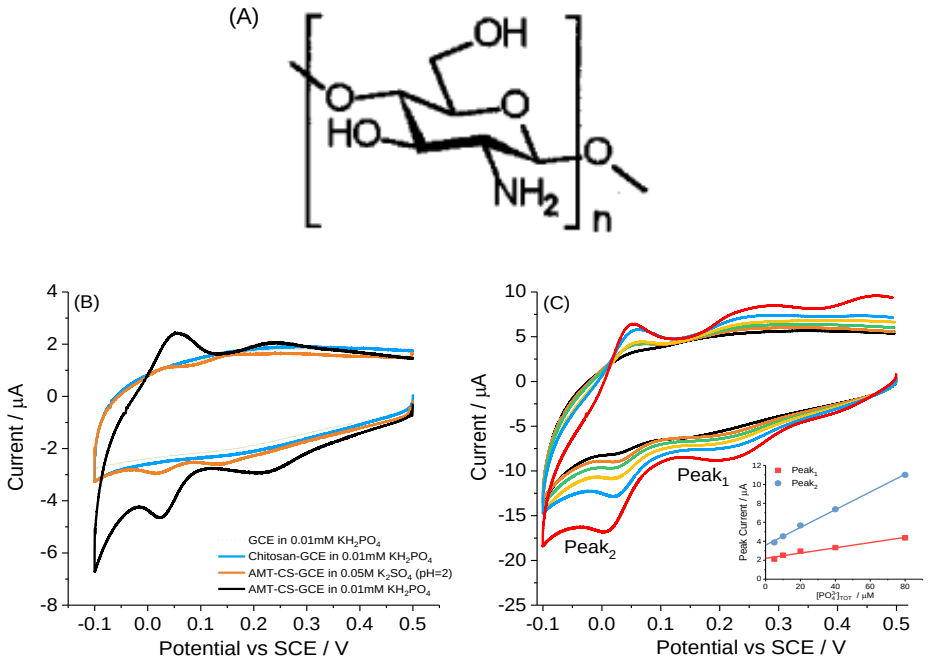

Figure.5 (A) The chemical structure of Chitosan; Reproduced from Chemical Reviews[33]. Copyright 2004 American Chemical Society (B) Electrochemical study of KH_2PO_4 at GC macroelectrodes at a scan rate of 100 mV s^{-1} under degassed condition: cyclic voltammograms of modified and unmodified GC macroelectrodes; (C) cyclic voltammetric responses of increasing concentration from 5.0–80.0 µM of KH_2PO_4 at AMT-CS-GCEs in 0.05 M K_2SO_4 (pH=2.0) (Inlay: calibration curve of peak current versus total phosphate concentration).

The sensitivity performance of modified electrode by square wave voltammetry. Before investigating the detection of phosphate by SWV, the analytical and voltammetric parameters such as accumulation time, scan rate and pulse height were optimized as described in the S8.

Next the SWV curves in varying concentrations of KH_2PO_4 and an AMT-CS-GCE were studied in 0.05M K_2SO_4 to determine the lower detectable level under two pH conditions (pH=2.0 and pH=5.8) separately (Fig.6). When the 0.05M K_2SO_4 solution pH was adjusted to 2.0, the peak heights of $Peak_1$ and $Peak_2$ at potentials of 0.20 V and 0.05V obtained at freshly prepared AMT-CS-GCEs within the detection range of 0.3-2.0 µM (Fig.6(A)) showed 'memory effects' since the adsorption of phosphate on the surface of modified electrode was almost fully irreversible with only slow desorption observed over very long timescales (Fig. S7). The linear relationships between $Peak_2$ current and phosphate concentration were described in Fig.6(B) by the following equation: $I_p(\mu A) = 4.38(\pm 0.12)\ [PO_4^{3-}]_{TOT}\ (\mu M) + 5.59(\pm 0.01)\ (\mu A)$, $R^2=0.9977$. The limit of detection (LOD) for

KH_2PO_4 was found to be 0.15 μM ($3\sigma_b/m$, n=10) with a sensitivity of 4.4(±0.1) μA/μM, signals were significantly amplified in SWV compared to CV. While concentrations exceeding 2.0 μM KH_2PO_4, the electrochemical signal in SWV started to level out as the adsorption sites on the surface of modified electrode and tended to saturate with KH_2PO_4 (Fig.S8(A)).

SWV by using AMT-CS-GCE was then conducted of KH_2PO_4 with the concentration in the range of 0.05–0.8 μM in 0.05M K_2SO_4 (measured pH=5.8) with three separate measurements for each concentration. Fig.6(C) showed the SWV response as a function of increasing concentration of KH_2PO_4. The plot of peak height of $Peak_2$ versus KH_2PO_4 concentration (Fig.6(D)) also indicated a linear relationship in the concentration range of 0.05–0.8 μM which could be depicted by a calibration curve $I_p(\mu A) = 6.53(\pm0.28)\ [PO_4^{3-}]_{TOT}\ (\mu M) + 2.53(\pm0.06)\ (\mu A)$, R^2=0.9908. The LOD was calculated to be 0.17 μM ($3\sigma_b/m$, n=10) of the blank by with a sensitivity of 6.5(±0.3) μA/μM. This result offered the experimental validation for the practicality of AMT-CS-GCE to detect the concentration of KH_2PO_4 sensitively with SWV technique under neutral condition. As displayed in Fig.S8(B), when the concentration of KH_2PO_4 was increased to 1.0 μM in 0.05M K_2SO_4 (pH=5.8), the linear relationship between $[PO_4^{3-}]_{TOT}$ and peak height of $Peak_2$ started to level out.

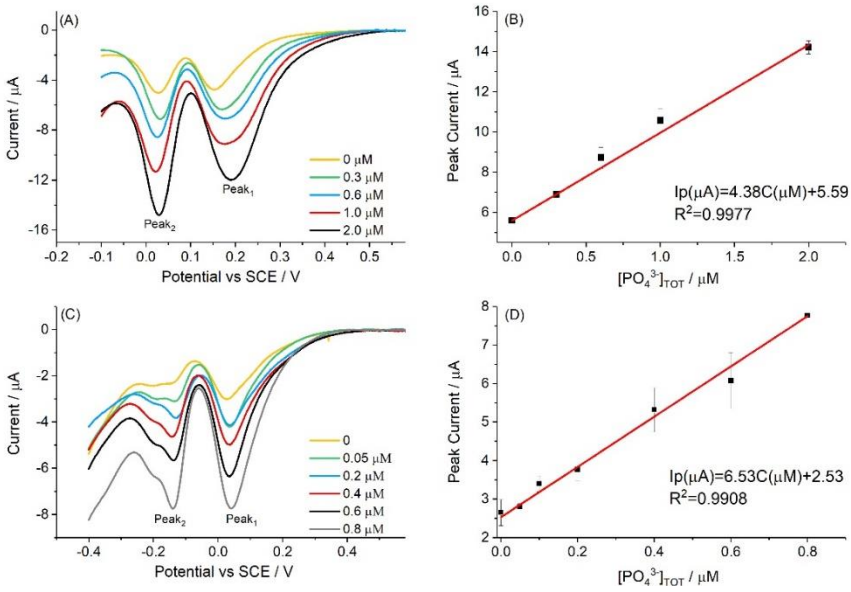

Figure.6 (A) Square wave voltammograms of AMT-CS-GCEs in 0.05M K_2SO_4 (pH=2) with varying concentrations of KH_2PO_4 from 0 μM to 2.0 μM and (B) calibration curve of $peak_2$ current versus total phosphate concentration; (C) Square wave voltammograms of AMT-CS-GCEs in 0.05M K_2SO_4 (pH=5.8) with varying concentration of KH_2PO_4 from 0 μM to 0.8 μM and (D) calibration curve of $peak_2$ current versus total phosphate concentration, scan rate =25 mVs^{-1}.

Interference testing and detection in real samples. Before applying AMT-CS-GCE for the detection of phosphate in real samples, the selectivity of the AMT-CS-GCE to phosphate was evaluated in the presence of Cl^- and NO_3^- separately (Fig. S9) since PO_4^{3-}, Cl^- and NO_3^- co-existed in most water environments[36, 37]. The SWV response of AMT-CS-GCE were first scanned in 0.05M K_2SO_4 (pH=2) in the presence of 0, 0.1 and 1 mM Cl^- or NO_3^- respectively in varying concentrations of KH_2PO_4 from 0 to 2.0 μM. The plot of current value of $Peak_2$ versus KH_2PO_4 concentration in the presence of 0, 0.1 and 1 mM Cl^- or NO_3^- visible in Fig.S9(A) and Fig.S9(B) respectively showed that the linear response to phosphate was unchanged to within 12% and 13% for concentrations of either chloride or nitrate of less than 1 mM which was markedly above the levels necessary for environmental analysis[38, 39]

Having investigated the inference from NO_3^- and Cl^- to the detection of KH_2PO_4 at AMT-CS-GCE, we next employed the SWV for the quantification of phosphate in real samples. The concentration of phosphate varies from 25 μg L^{-1} to 1.6 mg L^{-1} (0.26 μM to 16.8 μM) in natural and waste waters[2, 40]. WHO in 1980 concluded that there was no nutritional basis for the regulation of phosphorus levels in the drinking water supplies[41]. However, to control eutrophication, US EPA made the recommendation of a total phosphate concentration, $[PO_4^{3-}]_{TOT} < 0.025$ mg L^{-1} (0.26 μM) in reservoirs and a maximum permissible concentration of orthophosphate in river water is 0.1 mg L^{-1} (1.05 μM)[5]. Based on these conditions and recommended safety limits for phosphate in the water, it is suggested that the LOD of AMT-CS-GCE (0.15 μM) meets the requirements of analyzing the concentration of phosphate in authentic samples, as next confirmed experimentally.

After simple filtering to remove any particulate matter, samples of tap water and 10-fold diluted pond water solution were analysed directly after the addition of 0.05M K_2SO_4 (pH=2). SWV was then performed under the experimental parameters reported (See S8). The $peak_2$ heights were measured from square wave voltammograms of AMT-CS-GCEs in solution with tap water or 10-fold diluted pond water using the standard addition method as described in the Experimental section and employing a simple background correction to the voltammetry (Fig.S10). The accuracy of the electrochemical measurement was validated by a "recovery" test where known concentration (0.05, 0.15 and 0.35 μM) KH_2PO_4 standard solutions were used to add into tested electrolyte 0.05M K_2SO_4 (pH=2) prepared by the tap water and 10-fold diluted pond water solution respectively prior to square wave voltammetric measurements. The values close to 100% were attained as shown in Table 1.

To investigate the applicability of AMT-CS-GCEs in raw, undiluted samples, the detection of inorganic phosphate in pond water was conducted by exposing the AMT-CS-GCEs to neat pond water. SWV performed according to optimized experimental parameters and the square wave voltammetric response in original sample (pH=7.8) was first obtained, then spiked with 0.05, 0.08, 0.10 and 0.15 μM KH_2PO_4. The possible interference by chloride at similar pH were investigated first in 0.05M K_2SO_4 (pH=7.8) at AMT-CS-GCEs in the presence of 0, 0.1 and 1 mM Cl^- in variable concentrations of KH_2PO_4 from 0 to 0.2 μM (shown in SI 13), the results of which showed a good resilience towards chloride at a pH value similar to the neat pond water. Meanwhile, the concentration of chloride in the neat pond water was obtained to be 10.2 mg L^{-1} (0.29 mM) by a Ag^+ standard titration method[42], confirming a concentration compatible with the analysis of phosphate at AMT-CS-GCEs. As shown in Fig.7(A), the electrochemical signal $Peak_1$ and $Peak_2$ from SWV can be observed at 0.0 and -0.2 V. The linear relationships between $Peak_2$ current and added KH_2PO_4 concentration in pond water was described in Fig.7(B) by the following equation: $I_p(\mu A)=28.71(\pm2.53)\ [PO_4^{3-}]_{TOT}\ (\mu M) + 2.89(\pm0.22)\ (\mu A)$, $R^2=0.9772$，confirming the application of AMT-CS-GCEs for environmental monitoring.

Table.1 Concentrations analyzed by calibration curves in Fig.6 (B) of detected phosphate in tap water and pond water with standard solutions and the corresponding recoveries.

Solution	Measured Concentration using SWV /μM	Recovery/%
Tap water		
Original Sample	0.22±0.02	/
Sample+0.05 μM KH_2PO_4	0.28±0.01	110
Sample+0.15 μM KH_2PO_4	0.37±0.07	91
Sample+0.35 μM KH_2PO_4	0.57±0.04	100
Pond water		
Original Sample after diluted 10 times	1.11 ±0.01	/
Sample+0.05 μM KH_2PO_4	1.17 ±0.01	116
Sample+0.15 μM KH_2PO_4	1.26 ±0.02	92
Sample+0.35 μM KH_2PO_4	1.47 ±0.01	107

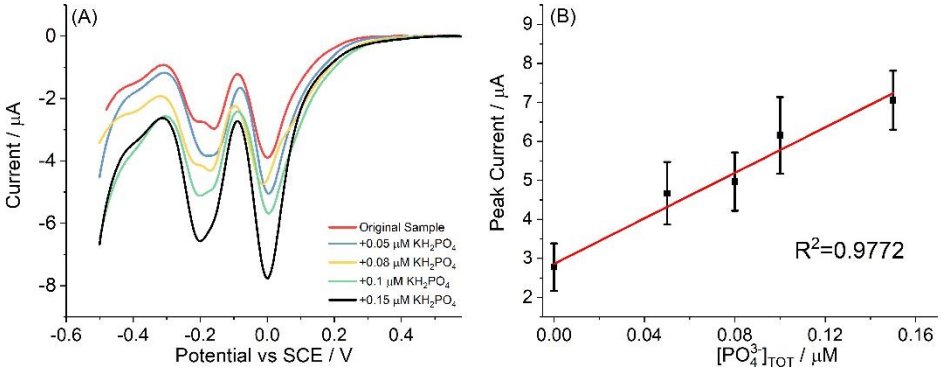

Figure.7 (A)Square wave voltammograms of AMT-CS-GCEs in pond water without any pre-treatment with varying concentrations of KH_2PO_4 from 0 μM to 0.15 μM and (B) calibration curve of $Peak_2$ current versus total phosphate concentration, scan rate=25 mVs^{-1}

■ CONCLUSIONS

The developed AMT-CS-GCE sensor realised a low detection limit for phosphate using cyclic voltammetry (CV) and square wave voltammetry (SWV), and showed high sensitivity of 4.4± 0.1μA/μM and selectivity in standard solutions and real samples. This kind of amperometric sensor is promising and practical for trace detection of inorganic phosphate in water environments in respect of the safety limits in drinking water and natural water set by US EPA.

■ ASSOCIATED CONTENT

The Supporting Information is available free of charge

Summary of phosphate detection methods using amperometric techniques, speciation of Mo (VI) in aqueous solution, calculation of Surface Coverage and Particle Average Separation, speciation of phosphate as a function of pH, species distribution of Mo and P containing compounds as a function of pH for various total phosphate concentrations, optimization of CV and SWV parameters, estimation of thickness of the chitosan layer, memory effects in AMT-CS-GCEs, the upper detection range of AMT-CS-GCE Interference test and the recovery test of AMT-CS-GCE in tap and pond water, the applicability of AMT-CS-GCE in 0.05M K_2SO_4 (pH=7.8) (PDF).

■ Author Information

Corresponding Author:

Richard G. Compton − Department of Chemistry, Physical and Theoretical Chemistry Laboratory,

Oxford University, Oxford OX1 3QZ, U.K.; orcid.org/0000-0001-9841-5041;

Email: richard.compton@chem.ox.ac.uk

Authors:

Yuanyuan Lu - Department of Chemistry, Physical and Theoretical Chemistry Laboratory, Oxford University, Oxford OX1 3QZ, U.K.

Xiuting Li − Institute for Advanced Study, Shenzhen University, Shenzhen, Guangdong 518060, China

Danlei Li − Department of Chemistry, Physical and Theoretical Chemistry Laboratory, Oxford University, Oxford OX1 3QZ, U.K.

Notes

The authors declare no competing financial interest.

■ ACKNOWLEDGEMENTS

The speciation modelling part in this study obtained much help from Dr. Bertold Rasche (Department of Chemistry, University of Cologne, Cologne, 50939, Germany, bertold.rasche@uni-koeln.de).

■ REFERENCE

1. Currie, D. J.; Kalff, J., The relative importance of bacterioplankton and phytoplankton in phosphorus uptake in freshwater 1. *Limnol Oceanogr* **1984,** *29* (2), 311-321.

2. Berchmans, S.; Issa, T. B.; Singh, P., Determination of inorganic phosphate by electroanalytical methods: A review. *Anal Chim Acta* **2012,** *729*, 7-20.

3. Chitrakar, R.; Tezuka, S.; Sonoda, A.; Sakane, K.; Ooi, K.; Hirotsu, T., Phosphate adsorption on synthetic goethite and akaganeite. *J Colloid Interf Sci* **2006,** *298* (2), 602-608.

4. Yao, W.; Millero, F. J., Adsorption of phosphate on manganese dioxide in seawater. *Environ Sci & Tech* **1996,** *30* (2), 536-541.

5. U.S. Environmental Protection Agency (EPA)., Water Quality Standards Handbook: Chapter 3: Water Quality Criteria. EPA Office of Water, Office of Science and Technology, Washington, DC.: **2017**.

6. Guo, Z.X.; Cai, Q.; Yang, Z., Determination of glyphosate and phosphate in water by ion

chromatography—inductively coupled plasma mass spectrometry detection. *J Chromatogr A* **2005,** *1100* (2), 160-167.

7. Silveira, E. L. C.; de Caland, L. B.; Tubino, M., Simultaneous quantitative analysis of the acetate, formate, chloride, phosphate and sulfate anions in biodiesel by ion chromatography. *Fuel* **2014,** *124*, 97-101.

8. Sarwar, M.; Leichner, J.; Naja, G. M.; Li, C. Z., Smart-phone, paper-based fluorescent sensor for ultra-low inorganic phosphate detection in environmental samples. *Microsyst & Nanoeng* **2019,** *5* (1), 1-10.

9. Kröckel, L.; Lehmann, H.; Wieduwilt, T.; Schmidt, M. A., Fluorescence detection for phosphate monitoring using reverse injection analysis. *Talanta* **2014,** *125*, 107-113.

10. Racicot, J. M.; Mako, T. L.; Olivelli, A.; Levine, M., A Paper-Based Device for Ultrasensitive, Colorimetric Phosphate Detection in Seawater. *Sensors* **2020,** *20* (10), 2766.

11. Chen, Y.C.; Lo, K.M.; Wang, Y.X.; Chiu, T.C.; Hu, C.C., A sensitive colorimetric probe for detection of the phosphate ion. *Sci Rep-UK* **2020,** *10* (1), 1-9.

12. Galhardo, C. X.; Masini, J. C., Spectrophotometric determination of phosphate and silicate by sequential injection using molybdenum blue chemistry. *Anal Chim Acta* **2000,** *417* (2), 191-200.

13. Snigur, D.; Chebotarev, A.; Bulat, K.; Duboviy, V., Fast room temperature cloud point extraction procedure for spectrophotometric determination of phosphate in water samples. *Anal Biochem* **2020,** *597*, 113671.

14. Farghaly, O. A.; Hameed, R. A.; Abu-Nawwas, A.-A. H., Analytical application using modern electrochemical techniques. *Int. J. Electrochem. Sci* **2014,** *9* (1), 3287-3318.

15. Cinti, S.; Talarico, D.; Palleschi, G.; Moscone, D.; Arduini, F., Novel reagentless paper-based screen-printed electrochemical sensor to detect phosphate. *Anal Chim acta* **2016,** *919*, 78-84.

16. Barus, C.; Romanytsia, I.; Striebig, N.; Garçon, V., Toward an in situ phosphate sensor in seawater using Square Wave Voltammetry. *Talanta* **2016,** *160*, 417-424.

17. Zhang, Z.; Jaffrezic-Renault, N.; Bessueille, F.; Leonard, D.; Xia, S.; Wang, X.; Chen, L.; Zhao, J., Development of a conductometric phosphate biosensor based on tri-layer maltose phosphorylase composite films. *Anal Chim Acta* **2008,** *615* (1), 73-79.

18. Upadhyay, L. S. B.; Verma, N., Alkaline phosphatase inhibition based conductometric biosensor for phosphate estimation in biological fluids. *Biosens Bioelectron* **2015,** *68*, 611-616.

19. Heineman, W. R.; Wieck, H. J.; Yacynych, A. M., Polymer film chemically modified electrode

as a potentiometric sensor. *Anal Chem* **1980,** *52* (2), 345-346.

20. De Marco, R., Determination of phosphate in hydroponic nutrient solutions using flow injection potentiometry and a cobalt-wire phosphate ion-selective electrode. *Talanta* **2003,** *60* (6), 1215-1221.

21. Zhu, L.; Zhou, X.; Shi, H., A potentiometric cobalt-based phosphate sensor based on screen-printing technology. *Front Env Sci & Eng* **2013,** *8* (6), 945-951.

22. Zeitoun, R.; Biswas, A., Electrochemical Mechanisms in Potentiometric Phosphate Sensing Using Pure Cobalt, Molybdenum and their Alloy for Environmental Applications. *Electroanal* **2020,** *33* (2), 421-430.

23. Kim, H.J.; Hummel, J. W.; Birrell, S. J.; Sudduth, K. A. In Evaluation of phosphate ion-selective membranes for real-time soil nutrient sensing, 2005 ASAE Annual Meeting, *American Society of Agricultural and Biological Engineers*: **2005**; 1.

24. Cacace, M.; Landau, E.; Ramsden, J., The Hofmeister series: salt and solvent effects on interfacial phenomena. *Q Rev Biophys* **1997,** *30* (3), 241-277.

25. Mirceski, V.; Skrzypek, S.; Stojanov, L., Square-wave voltammetry. *ChemTexts* **2018,** *4* (4), 1-14.

26. Puigdomenech, I., Hydra/Medusa chemical equilibrium database and plotting software. *KTH Royal Institute of Technology* **2004**.

27. Pettersson, L.; Andersson, I.; Oehman, L. O., Multicomponent polyanions. 39. Speciation in the aqueous hydrogen ion-molybdate (MoO_4^{2-})-hydrogenphosphate (HPO_4^{2-}) system as deduced from a combined Emf-phosphorus-31 NMR study. *Inorg Chem* **1986,** *25* (26), 4726-4733.

28. Evans, H. T.; Gatehouse, B. M.; Leverett, P., Crystal structure of the heptamolybdate (VI)(paramolybdate) ion, $[Mo_7O_{24}]^{6-}$, in the ammonium and potassium tetrahydrate salts. *Journal of the Chemical Society, Dalton Transactions* **1975,** (6), 505-514.

29. Ilangovan, G.; Pillai, K. C., Mechanism of activation of glassy carbon electrodes by cathodic pretreatment. *J Solid State Electr* **1999,** *3* (6), 357-360.

30. Pillai, K. C.; Ilangovan, G., Cyclic voltammetric studies of electroreduction of Mo (VI) on glassy carbon electrode. *Bulletin of Electrochemistry* **1993,** *9* (11), 592-595.

31. Parsons, R., *Standard Electrode Potentials, Units, Conventions, and Methods of Determination*. 2017; Vol. 1, 1-11.

32. Unoura, K.; Tanaka, N., Comparative study of the electrode reactions of 12-molybdosilicate and 12-molybdophosphate. *Inorg Chem* **1983,** *22* (20), 2963-2964.

33. Kumar, M N V R.; Muzzarelli, R A A.; Muzzarelli, C.; Domb, A J., Chitosan chemistry and pharmaceutical perspectives. *Chem. Rev* **2004**, *104*(12): 6017-6084.

34. Rinaudo, M.; Pavlov, G.; Desbrieres, J., Influence of acetic acid concentration on the solubilization of chitosan. *Polymer* **1999,** *40* (25), 7029-7032.

35. Congur, G.; Eksin, E.; Erdem, A., Chitosan modified graphite electrodes developed for electrochemical monitoring of interaction between daunorubicin and DNA. *Sensing and Bio-Sensing Research* **2019,** *22*, 100255.

36. Ewaid, S. H.; Abed, S. A., Water quality index for Al-Gharraf river, southern Iraq. *The Egyptian Journal of Aquatic Research* **2017,** *43* (2), 117-122.

37. Bahroun, S.; Chaib, W., The quality of surface waters of the dam reservoir Mexa, Northeast of Algeria. *Journal of Water and Land Development* **2017**.

38. Ozoko, D.; Onyeabor, C., Water Quality Assessment of Ugwueme surface and ground water system. *International Journal of Science and Research* **2017,** *6* (9), 833-838.

39. Adejumo, R.; Adagunodo, T.; Bility, H.; Lukman, A.; Isibor, P. O., Physicochemical constituents of groundwater and its quality in crystalline bedrock, Nigeria. *International Journal of Civil Engineering and Technology (IJCIET)* **2018,** *8* (9), 887-903.

40. Bartram, J.; Thyssen, N.; Gowers, A., *Water and health in Europe: a joint report from the European Environment Agency and the WHO Regional Office for Europe*. WHO Regional Office Europe: 2002.

41. Edition, F., Guidelines for drinking water quality. *WHO chronicle* **2011,** *38* (4), 104-108.

42. Federation, W. E.; Association, A., Standard methods for the examination of water and wastewater. *American Public Health Association (APHA): Washington, DC, USA* **2005**.

■ TABLE OF CONTENTS GRAPHIC: